Supplementary Methods

MRI acquisition

The same imaging protocol was applied to all participants (patients and controls). Images were acquired on a Siemens 3T Verio MRI scanner equipped with a 12-channel head coil. The imaging protocol yielded a high-resolution T1-weighted image, with an isotropic voxel size of 1 mm (TR=2250 ms, TE=41 ms, FOV = 256x256 mm^2). Diffusion-weighted images were obtained using two diffusion weightings (b = 0 and 1000 s/mm^2) along 30 diffusion-encoding directions (TR = 10,600 ms, TE = 100 ms, FOV = 224×224 mm^2, parallel imaging factor of 2, slice thickness = 2 mm, and 60 axial slices, isotropic voxel size of 3 mm).

Image processing

DICOM images were converted to NIfTI format (with extraction of diffusion gradient directions) using the software dcm2nii, part of the software suite MRIcron (http://www.mccauslandcenter.sc.edu/mricro/mricron/dcm2nii.html). The package FMRIB Software Library (FSL)'s Diffusion Toolkit (FDT) (www.fmrib.ox.ac.uk/fsl) was used for preprocessing diffusion-weighted images and for diffusion tensor estimation[1, 2]. The images underwent eddy current correction through affine transformation of each DWI to the base b = 0, T2-weighted image.

White matter fiber tract reconstruction

Probabilistic tractography was used to define the number of white matter streamlines connecting cortical regions, which were separately defined according to an anatomical atlas. This step was iteratively performed until the connectivity between all

possible pairs of cortical regions was determined. The connectivity information was then compiled in a connectivity matrix, providing a two-dimensional representation of the brain connectome. These steps are explained in detail below. We employed probabilistic connectivity in this study, even though it is more time-consuming technique, since it can provide a more comprehensive view of the distributions of the numbers of streamlines across nodes[1, 3], therefore mitigating network sparsity, particularly given our relatively small sample size.

Structural connectivity was obtained by applying FDT's probabilistic method for fiber tracking[1, 3, 4]. Probabilistic tractography was performed on diffusion data after voxel-wise calculation of the diffusion tensor. FDT's BEDPOST was used to build default distributions of diffusion parameters at each voxel. Probabilistic tractography was obtained using FDT's probtrackx with 5000 individual streamlines drawn through the probability distributions on principal fiber direction. We chose to employ probabilistic tractography in this study, since it is theoretically capable of accommodating intra-voxel fiber crossings[1, 5].

Cortical seed regions for tractography were obtained from an automatic segmentation process employing FreeSurfer (http://surfer.nmr.mgh.harvard.edu/) applied to T1 weighted images. This process subdivides the human cerebral cortex into sulco-gyral based cortical and subcortical regions of interest (ROIs) by automatically assigning a neuroanatomical label to each location on a cortical surface model based on probabilistic information estimated from a manually labeled training set (the Lausanne anatomical atlas, distributed as part of the Connectome Mapping Toolkit

[http://www.connectome.ch][6]), yielding 82 ROIs in the subjects' native T1-weighted space (41 regions in each hemisphere). All processed images were visually inspected to ensure cortical segmentation quality. The ROIs were transformed into each subject's DTI space using an affine transformation obtained with FSL's FLIRT. Probabilistic tractography was performed using each of the 82 cortical ROIs in diffusion space as the seed region.

Individual connectome reconstruction

For each subject, we calculated the connectivity between cortical ROIs i and j defined as the number of probabilistic white matter streamlines arriving at j when i was seeded, averaged with the number of probabilistic streamlines arriving at i when j was seeded. The step was iteratively repeated to ensure that all 82 cortical ROIs were used as seed regions. Once all iterations were completed, a connectivity matrix A was constructed, with 82x82 entries, where each entry A_{ij} corresponded to the weighted connectivity between structures i and j, also referred to as the link between nodes i and j. Since the number of streamlines between i to j, and j to i were averaged, the connectivity matrix was symmetrical with respect to its main diagonal.

The connectivity matrices from patients were then normalized based on the connectivity matrices from controls. For each patient, a connectivity matrix Z was constructed where the link Z_{ij} corresponded to the Z score of the patient's link A_{ij} relative to the equivalent link (between ROIs i and j) among controls. Specifically, for each specific link, the Z score was calculated as the number of standard deviations away

from the mean, where the standard deviation and the mean were obtained from the control distribution.

The use of link-wise Z scores was preferred here, since it may enable the independent subsequent testing of our hypothesis, as by comparing patients with a local distribution of controls, researchers may obtain a normalization of patient connectomes, enabling the comparison or grouping of patients across sites.

Link selection based on anatomy of medial temporal lobe connectivity.

In order to examine the predictive value of neural network architecture towards surgical outcome, we focused our analyses on links connecting the medial temporal region (ipsilateral to seizure onset) with the rest of the brain. This step represented a "hand-design" component of feature selection for our model based on the anatomical premise of our hypothesis, which suggested that patients not seizure-free would exhibit consistent differences in connectivity (compared with controls) between temporal structures and areas not typically resected during surgery. Of note, it is possible that abnormal epileptogenic networks may be exclusively located outside the temporal lobe and not involve temporal regions. These networks were not tested in this study. We focused on temporal-extra-temporal structures given the pre-surgical neurophysiological evidence of temporal lobe involvement of ictal onset on all patients.

The temporal regions were (in accordance with the Lausanne anatomical atlas referenced above): parahippocampal gyrus; entorhinal cortex; temporopolar region; inferior, middle and superior temporal gyri; hippocampus; and amygdala). Only links connecting temporal lobe regions with other brain regions were included. Links

between non- temporal regions, or within temporal regions were therefore excluded. Given that there were overall 82 anatomical regions, there were 592 possible links between medial temporal regions and the rest of the brain (8 medial temporal regions x 74 remaining brain regions). All subsequent analyses were based on this set of links. This step was performed to reduce the number of features of the predictive model (therefore aiming to avoid overfitting) focusing only on regions located anatomically in accordance with our biological hypothesis that neural network architecture associated with surgical outcome is likely to be related to connectivity of the temporal lobe.

Across these 592 links, controls exhibited 2.571±1.103 % of links with Z score >2 (compared with other controls), ranging from 0.18% to 4.89%. All links were measured in all controls.

Assessment of sub-network sizes

A score composed of the number of links with a Z score higher than Z=2 was obtained for multiple sub-network sizes. A vector was obtained composed of links 1 to n representing the Z scores of links sorted by AUC. This vector was binarized (if Z>2, =1, otherwise =0), and the sum of all elements in each vector was obtained, yielding a score per patient. The step above was performed repeatedly with sub-networks ranging from 1 to 50 links sorted based on AUCs as described above, in order to assess the predictive value across a variable range of sub-network sizes. The arbitrary threshold of 50 links was chosen since we hypothesized that abnormal subnetworks would encompass sub-networks with fewer than 50 links. For each sub-network size, the overall model AUC was calculated based on the network score. The point of maximal accuracy of the AUC

was determined based on the network score threshold where the sum of sensitivity and specificity was maximal. For this network score threshold, the predictive values towards seizure-free and not seizure-free outcomes were calculated. For example, for a given sub-network size, the maximal accuracy could be achieved by a network score of 5, indicating that patients with less than 5 links with a Z score greater than 2 in the sub-network were more likely to achieve seizure-freedom.

We tested the accuracy of the model by repeating the steps above with resampling with replacement (bootstrapping) the entire analytic approach described above, where patient and controls were resampled and yielding new individual scores. For each resample, we calculated the model AUC to assess confidence intervals.

Model from clinical data

The following clinical variables were analyzed: age of onset of epilepsy, age at surgery, seizure frequency (including complex partial seizures or secondarily generalized seizures), duration of epilepsy, seizure burden (here defined as duration of epilepsy multiplied by seizure frequency), side of TLE, presence of hippocampal atrophy on diagnostic pre-surgical MRI, pre-surgical interictal epileptiform EEG findings (ipsilateral to seizure onset only, contralateral to seizure onset only, bilateral or none) and epilepsy risk factors (history of traumatic brain injury, central nervous system infection or febrile seizures). For continuous variables, each subject's score was defined based on the variable value. For categorical values (e.g., history of febrile seizures), each subject's score was defined as a binary variable indicating absence or presence of the clinical variable. After ROCs were constructed for each clinical variable, a point in the ROC

corresponding to the variable threshold of maximal accuracy was defined, and sensitivity, specificity and predictive values corresponding to this threshold were defined. We also assessed a model comprised of clinical variables, where each subject received a score defined based on the cumulative weight of clinical measures. In this model, each continuous clinical variable above was assessed regarding its threshold of maximal accuracy. Numbers above this threshold were counted as 1 (otherwise as 0) in case of age at surgery, seizure frequency, and epilepsy duration and seizure burden. In the case of age of onset, scores below the threshold were counted as 1. In this model, lack of hippocampal atrophy, bilateral or contralateral interictal EEG abnormalities and presence of any risk factors were independently counted as 1 (otherwise as 0). For each subject, a composite score based on this clinical model was obtained by summing the binary scores described above; higher scores indicating a higher number of potential predictors of a not seizure-free outcome.

Figure e-1- Adjacency matrices demonstrating link-wise Z scores in patients, relative to control subjects. Links 1-41 represent ROIs in the contralateral hemisphere, while links 42-82 represent links in the hemisphere ipsilateral to seizure onset.

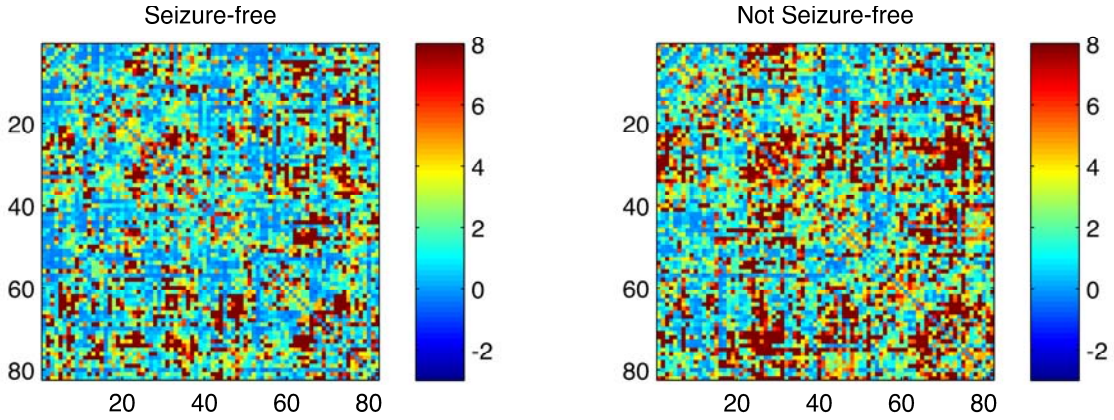

Table e-1 - Demographic and clinical information from the patients studied in this manuscript. Sz= Seizure; L ATL= left anterior temporal lobectomy; R ATL= right anterior temporal lobectomy; M=male; F= female; Ipsilateral= ipsilateral to side of TLE; Contralateral= contralateral to side of TLE; SF = seizure-free; NSF= not seizure-free, F=female, M=male. The second row demonstrates the statistical comparison of the distributions of each variable between the seizure-free versus non-seizure-free groups.

Patient No.	***Age of epilepsy onset (years)***	***Surgery type***	***Age at Surgery***	***Gender***	***Risk Factors***	***Interictal EEG***	***Sz frequency***	***Epilepsy duration***	***Sz burden***	***Months since surgery***	***Surgery Outcome***
SZ vs NSF	***t(33)=0.82, p=0.42***	***Yates' Chi(1)=0.021,p=0.88***	***t(33)=0.68, p=0.5***	***Yates' Chi(1)=0.01,p=0.9***	***Yates' Chi(1)=0.77,p=0.38***	***Yates' Chi(1)=0.31,p=0.58***	***t(33)=-0.26, p=0.79***	***t(33)=-0.49, p=0.63***	***t(33)=-0.68, p=0.89***	***t(33)=1.45, p=0.23***	
1	0.5	L ATL	43.76	M	Infection, TBI	Ipsilateral	30	37.88	1136.4	14	Not SF
2	15	L ATL	50.53	M	TBI	Ipsilateral	192	29.68	5698.56	16	Not SF
3	23	L ATL	41.47	F	None	Ipsilateral	48	14.04	673.92	21	Not SF
4	20	L ATL	67.07	M	TBI	Ipsilateral	24	41.97	1007.28	32	Not SF
5	27	L ATL	50.48	F	None	Bilateral	12	18.47	221.64	22	Not SF
6	47	L ATL	54.83	F	Infection	Bilateral	24	3.48	83.52	22	Not SF
7	1	L ATL	25.64	F	None	None	48	18.53	889.44	32	Not SF
8	19	R ATL	32.11	M	None	Contralateral	30	7.65	229.5	15	Not SF
9	13	R ATL	26.49	F	None	None	36	9.01	324.36	17	Not SF
10	20	R ATL	55.44	F	None	Ipsilateral	12	30.82	369.84	20	Not SF
11	34	R ATL	45.61	F	None	Bilateral	24	4.68	112.32	31	Not SF
12	1.5	R ATL	52.21	F	Infection	Ipsilateral	36	46.42	1671.12	13	Not SF
13	24	R ATL	45.01	F	None	Ipsilateral	900	16.51	14859	19	Not SF
14	13	R ATL	58.07	M	TBI	None	24	38.2	916.8	20	Not SF
15	62	R ATL	73.11	F	None	Bilateral	48	6.73	323.04	25	Not SF
16	26	R ATL	39.58	M	None	Bilateral	192	8.39	1610.88	36	Not SF
17	39	R ATL	54.82	F	None	Ipsilateral	120	11.15	1338	38	Not SF
18	30	L ATL	47.76	M	TBI	None	15.6	12.85	200.46	35	SF
19	15	L ATL	56.59	F	Infection	Ipsilateral	102	37.24	3798.48	32	SF
20	1.33	L ATL	49.46	F	Febrile seizure	Bilateral	60	43.79	2627.4	13	SF
21	0.75	L ATL	42.73	F	Febrile seizure	Ipsilateral	144	37.16	5351.04	14	SF
22	8	L ATL	48.87	F	TBI	Ipsilateral	18	36.43	788.22	15	SF
23	44	L ATL	54.51	F	None	Ipsilateral	900	5.39	4851	17	SF
24	40	L ATL	50.35	F	None	Bilateral	120	5.88	705.6	38	SF
25	12	L ATL	41.06	F	Infection	Bilateral	24	24.31	583.44	17	SF

26	47	R ATL	55.15	F	None	Ipsilateral	18	4.03	72.54	18	SF
27	18	R ATL	34.76	F	None	Ipsilateral	240	12.49	2997.6	20	SF
28	20	R ATL	40.25	F	None	Bilateral	24	15.75	378	21	SF
29	1	R ATL	25.83	M	Febrile seizure	Ipsilateral	132	20.35	2686.2	13	SF
30	5	R ATL	55.83	F	None	Bilateral	144	46.06	6632.64	31	SF
31	5	R ATL	46.7	M	None	Bilateral	8.04	37.2	299.09	30	SF
32	37	R ATL	43.53	F	None	Bilateral	120	2.39	286.8	45	SF
33	20	R ATL	28.54	F	None	Contralateral	60	4.24	254.4	13	SF
34	12	R ATL	45.5	M	TBI	Ipsilateral	48	28.26	1356.48	16	SF
35	13	R ATL	51.15	M	Febrile seizure	Bilateral	54	33.64	1816.56	19	SF

References to the Supplementary Materials

1. Behrens TE, Berg HJ, Jbabdi S, Rushworth MF, Woolrich MW. Probabilistic diffusion tractography with multiple fibre orientations: What can we gain? Neuroimage 2007;34:144-155.
2. Heiervang E, Behrens TE, Mackay CE, Robson MD, Johansen-Berg H. Between session reproducibility and between subject variability of diffusion MR and tractography measures. Neuroimage 2006;33:867-877.
3. Behrens TE, Woolrich MW, Jenkinson M, et al. Characterization and propagation of uncertainty in diffusion-weighted MR imaging. Magn Reson Med 2003;50:1077-1088.
4. Ciccarelli O, Behrens TE, Altmann DR, et al. Probabilistic diffusion tractography: a potential tool to assess the rate of disease progression in amyotrophic lateral sclerosis. Brain 2006;129:1859-1871.
5. Nucifora PG, Verma R, Lee SK, Melhem ER. Diffusion-tensor MR imaging and tractography: exploring brain microstructure and connectivity. Radiology 2007;245:367-384.
6. Gerhard S, Daducci A, Lemkaddem A, Meuli R, Thiran JP, Hagmann P. The connectome viewer toolkit: an open source framework to manage, analyze, and visualize connectomes. Frontiers in neuroinformatics 2011;5:3.